iScience

CellPress
OPEN ACCESS

Article

Fluid-driven hydrogel actuators with an origami structure

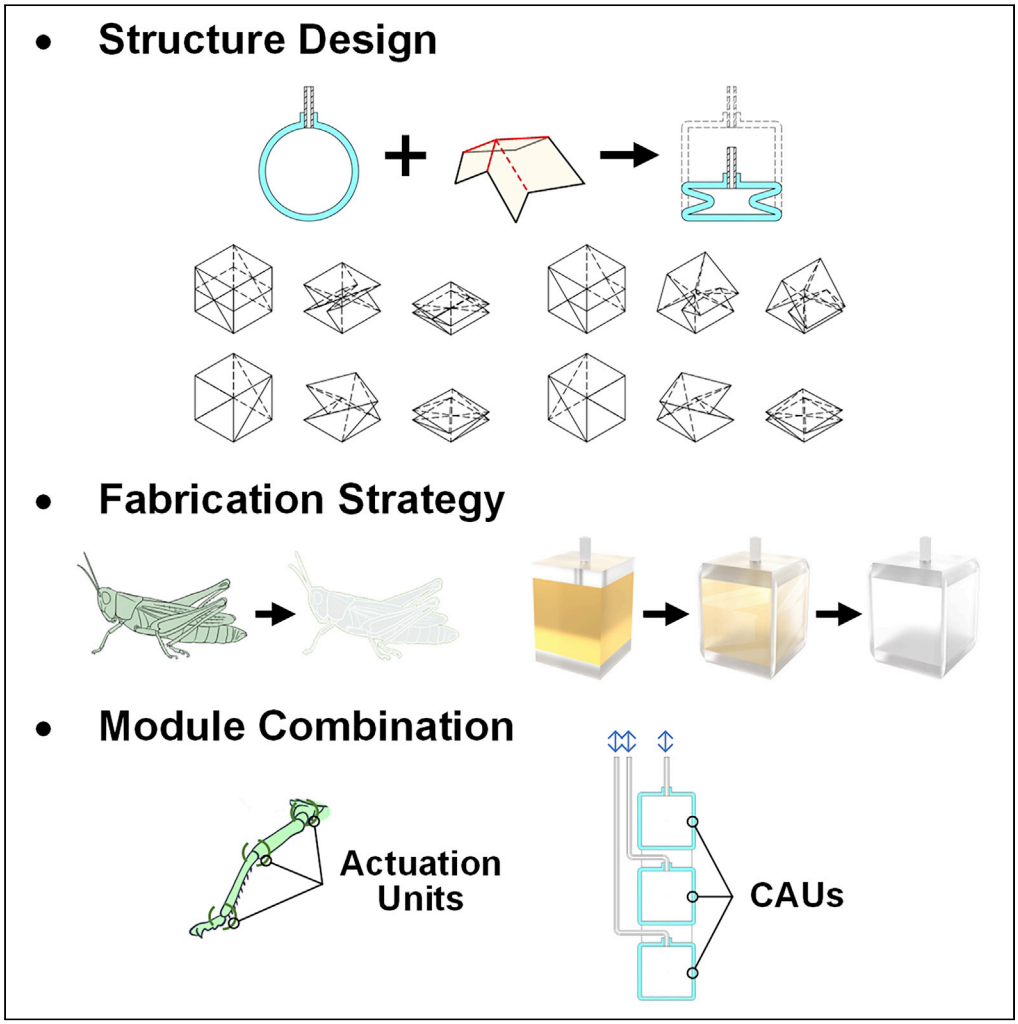

Zhexin Huang, Cunyue Wei, Lina Dong, Anyang Wang, Hongyi Yao, Zhongwei Guo, Shengli Mi

guozw2020@sz.tsinghua.edu.cn (Z.G.)
mi.shengli@sz.tsinghua.edu.cn (S.M.)

Highlights

Origami structures were introduced to fluid-driven hydrogel actuators

Three types of cuboid actuator units (CAUs) achieved linear motion, bending, and twisting

A fabrication strategy was based on removable templates and *in situ* formation

Combinations of multiple CAUs achieved different actuation modes

Huang et al., iScience *25*, 104674
July 15, 2022 © 2022
https://doi.org/10.1016/j.isci.2022.104674

iScience

CellPress
OPEN ACCESS

Article

Fluid-driven hydrogel actuators with an origami structure

Zhexin Huang,[1,2] Cunyue Wei,[1] Lina Dong,[1,3] Anyang Wang,[1,2] Hongyi Yao,[1,2] Zhongwei Guo,[1,3,*] and Shengli Mi[1,2,4,*]

SUMMARY

Owing to the innate good biocompatibility, tissue-like softness and other unique properties, hydrogels are of particular interest as promising compliant materials for biomimetic soft actuators. However, the actuation diversity of hydrogel actuators is always restricted by their structure design and fabrication methods. Herein, origami structures were introduced to the design of fluid-driven hydrogel actuators to achieve diverse actuation movements, and a facile fabrication strategy based on removable templates and inside-out diffusion-induced *in situ* hydrogel crosslinking was adopted. As a result, three types of modular cuboid actuator units (CAUs) achieved linear motion, bending, and twisting. Moreover, combinations of multiple CAUs achieved different actuation modes, including actuation decoupling, superposition, and reprogramming. The diverse actuation functionality would enable new possibilities in application fields for hydrogel soft actuators. Several simple application demos, such as grippers for grasping tasks and a multi-way circuit switch, demonstrated their potential for further applications.

INTRODUCTION

In nature, biological actuation systems, especially the musculoskeletal systems of animals, perform complex movements with high adaptability and compliance, including linear motion (elongation & contraction), twisting, bending, and more complex combinations of them (Coyle et al., 2018). Taking inspiration from them, biomimetic soft actuators, as one of the main components of soft robots, aim to reproduce these biological actuations to carry out more varied tasks with higher flexibility, environmental compliance, and safety in human-machine interfaces and machine-environment interactions, than conventional rigid actuators (Shen, 2021; Ilami et al., 2021).

Hydrogels, due to their innate good biocompatibility, tissue-like softness and flexibility, are of particular interest as a kind of promising compliant materials for biomimetic soft actuators (Liu et al., 2020; Lee et al., 2020; Jiao et al., 2022), especially in biological applications (Banerjee et al., 2018). They are composed of hydrophilic 3D crosslinked polymer networks and aqueous solutions, possessing distinct characteristics superior to those of conventional elastic materials (e.g. silicone elastomers) for biomimetic soft robotics, such as high water content, biodegradability, transparency, ionic conductivity, stimulus-responsiveness, and diversity of physicochemical characteristics (Ionov, 2014; Ding et al., 2020; Liu et al., 2020; Lee et al., 2020). Benefiting from these excellent characteristics, hydrogel actuators have great strengths and potential in a wide variety of application fields (Shang et al., 2019; Le et al., 2019), including soft machines and robotics (Han et al., 2018; Li et al., 2020; Downs et al., 2020; Zhu et al., 2020), artificial muscles (Park and Kim, 2020), biomedical engineering (Shim et al., 2012), microfluidic devices (D'eramo et al., 2018), optical devices (Duan et al., 2017), and so on.

Existing osmotic-driven hydrogel actuators always have the disadvantages of low actuation speed and/or low actuation force (Yuk et al., 2017; Liu et al., 2020; Jiao et al., 2022). Fluid-driven (hydraulic or pneumatic) actuation (Zhang et al., 2020), the most widely used actuation method for soft actuators due to its simplicity, low cost, safety, large actuation force, and high energy efficiency, is a promising method to address this problem by introducing chambers and channels inside hydrogels (Yuk et al., 2017; Liu et al., 2020). A type of hydraulic hydrogel actuator was first reported by Yuk et al. (Yuk et al., 2017). Since then, researchers have exploited the unique material properties of hydrogels to endow fluid-driven soft actuators various innovative functions, such as high transparency for optical and sonic camouflage in water (Yuk et al.,

[1]Bio-manufacturing Engineering Laboratory, Tsinghua Shenzhen International Graduate School, Tsinghua University, Shenzhen 518000, Guangdong, China

[2]Department of Mechanical Engineering, Tsinghua University, Beijing 100084, China

[3]Macromolecular Platforms for Translational Medicine and Bio-Manufacturing Laboratory, Tsinghua-Berkeley Shenzhen Institute, Shenzhen 518055, Guangdong, China

[4]Lead contact

*Correspondence: guozw2020@sz.tsinghua.edu.cn (Z.G.), mi.shengli@sz.tsinghua.edu.cn (S.M.)

https://doi.org/10.1016/j.isci.2022.104674

This is an open access article under the CC BY-NC-ND license (http://creativecommons.org/licenses/by-nc-nd/4.0/).

2017), biodegradability and sustainability (Shintake et al., 2017), thermal-responsiveness for thermoregulation (Mishra et al., 2020; Mishra et al., 2021), and ionic conductivity for soft sensing (Hardman et al., 2022).

However, on the one hand, as a result of the lack of structural diversity, most existing fluid-driven hydrogel actuators (Yuk et al., 2017; Shintake et al., 2017; Zhang et al., 2018; Mishra et al., 2020; Mishra et al., 2021; Takishima et al., 2021; Hardman et al., 2022) can only perform a simple bending actuation, which would limit their further applications in practice. Baumgartner et al. applied a textile exoskeleton to direct the bending actuation (Baumgartner et al., 2020). On the other hand, the structural diversity of hydrogel actuators is always limited by current fabrication methods for the preparation of complex 3D thin-walled hollow hydrogel structures with chambers and channels, such as molding (Yuk et al., 2017; Shintake et al., 2017). Benefiting from 3D printing methods for hydrogels, Cheng et al. (Cheng et al., 2019) and Heiden et al. (Heiden et al., 2022) realized multidirectional bending actuation through a multiple-chamber structure. However, 3D printing methods for hydrogels always require specialized printers, and there are only limited ink materials with applicable crosslinking networks can be used, which restrict their wide applications (Wu et al., 2019; Hardman et al., 2022). A few studies have proposed a simple *in situ* forming method based on inside-out diffusion-induced polymerization of hydrogels (Yu et al., 2019) or other polymers (Subraveti and Raghavan, 2021), and some studies have applied this method with removable templates to form hollow hydrogel structures (Ma et al., 2018b; Ma et al., 2018a; Lin et al., 2019). Wu et al. adopted this method to fabricate bellow-shaped fluid-driven hydrogel actuators (Wu et al., 2019).

Origami structures, due to their inflatable and foldable structures, have been introduced to the design of fluid-driven soft actuators to obtain various desired actuation movements (e.g., linear motion (Li et al., 2017; Lin et al., 2020), bending (Li et al., 2017; Lin et al., 2020; Jiao et al., 2021; Göttler et al., 2021), twisting (Li et al., 2017; Jiao et al., 2021), and other complex actuation (Kim et al., 2019; Li et al., 2019)) and/or achieve a larger deformation ratio (Lee and Rodrigue, 2019). However, the design of the origami structures always poses manufacturing difficulties, and to the best of our knowledge, no type of fluid-driven hydrogel actuators has yet been proposed with an origami structure.

Herein, a type of fluid-driven hydrogel actuators with origami structures is designed, and a simple fabrication method based on removable templates and inside-out diffusion-induced *in situ* crosslinking is adopted to construct such a kind of complex 3D thin-walled hollow hydrogels with origami structures in one piece. Origami structures with a predesigned crease pattern guide the directional movements of fluid-driven hydrogel actuators when they are actuated. Three basic types of modular actuator units of linear motion, bending, and twisting, were designed, fabricated, and tested, which are hereafter referred to as cuboid actuator units (CAUs) due to their cuboid shapes. Moreover, with the modular design thinking, combinations of multiple CAUs are capable of achieving combinations of actuation, such as motion decoupling and superposition. Each CAU was independently controlled to actuate, and different actuation sequences and combinations of actuation states of CAUs achieved on-demand spatiotemporal actuations and reprogramming of shape changes. Finally, several simple application demos for different tasks were demonstrated, such as a two-finger gripper and a three-finger gripper for grasping tasks, and a multi-way circuit switch.

RESULTS

Design concept of CAUs

Herein, origami structures are introduced to fluid-driven hydrogel actuators to achieve more diverse actuation movements. Three types of cuboid actuator units (CAUs) are designed, which are basic actuator modules of linear motion, bending, and twisting: linear-contraction cube (LCC), tilting-bending cube (TBC), and twisting-contraction cube of clockwise and counter-clockwise directions (TCC-CW & TCC-CCW), respectively. Their crease patterns and folding kinematics are shown in Figures 1B–1E. Solid lines represent mountain creases, and dotted lines represent valley creases. Among them, an LCC performs a unidirectional elongation-contraction motion, a TBC performs a tilting motion, which can be further transformed into a bending motion, and a TCC performs a coupled motion of twisting and linear motion.

For a cuboid soft actuator without creases, as shown in Figure 1A i, its four side faces deform inward equally to form concavities under an applied negative fluid pressure. Because the four side faces have the same and symmetric shape, their deformation is identical to each other and symmetric within each of them,

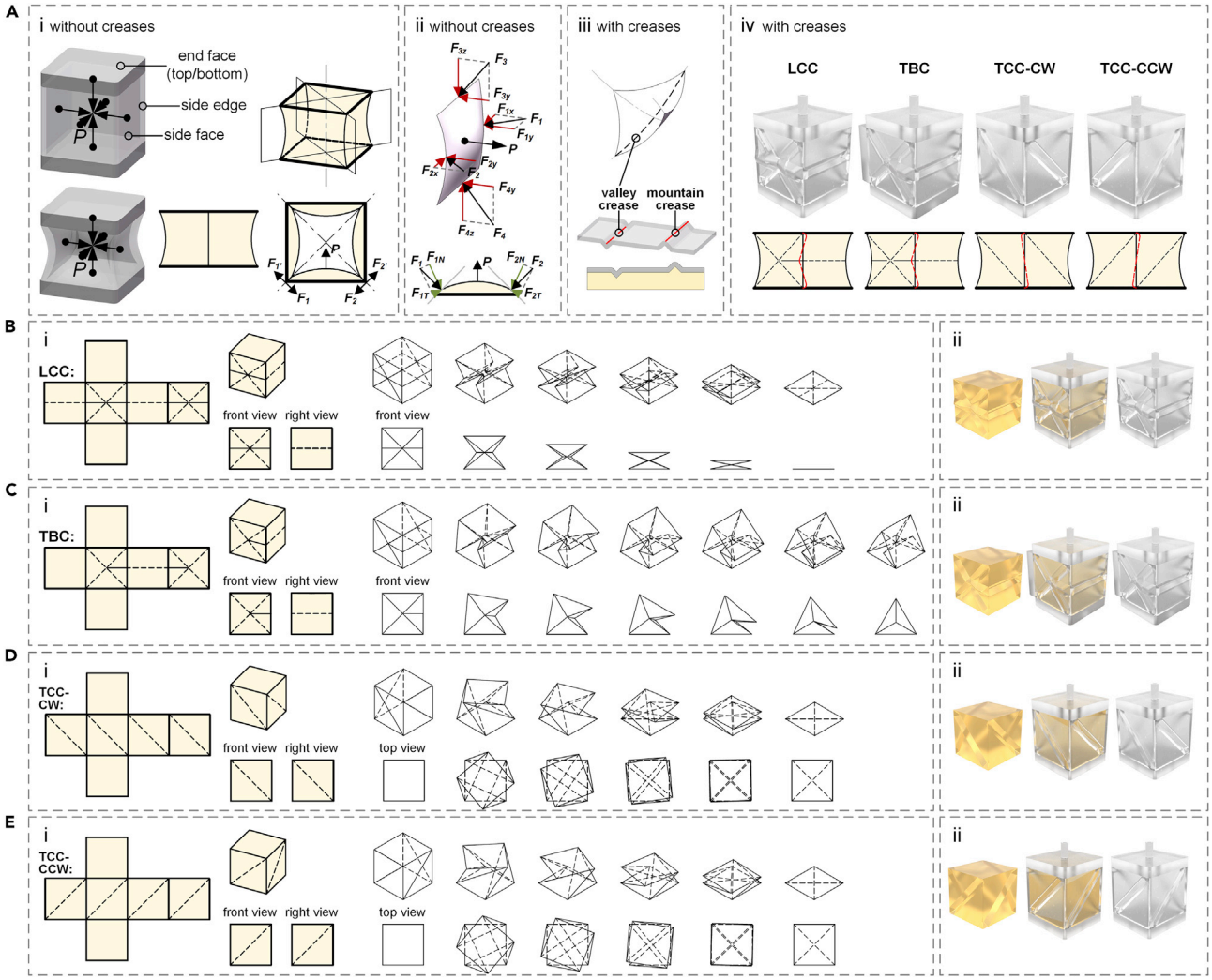

Figure 1. Design concept of CAUs

(A) Mechanism of origami structures on CAUs: i. For a cuboid soft actuator without creases, its four side faces deform inward equally to form concavities under an applied negative fluid pressure. ii. For each side face, a pressure *P* and forces on its four edges produces bending deformation and compressive deformation. iii. Due to a crease structure, a face tends to bend in the direction perpendicular to the crease lines when a negative pressure is applied. iv. The crease structures also bring a local stiffness difference at each side edge and make it incline when actuated.

(B–E) The designs of LCC, TBC, TCC-CW, and TCC-CCW: i. Crease pattern designs and folding kinematics of LCC, TBC, TCC-CW, and TCC-CCW. ii. Structure designs of LCC, TBC, TCC-CW and TCC-CCW, and their cores. See also Figure S2.

and the side edge between each pair of adjacent side faces bends inward on the symmetry plane of the two adjacent side faces. For each side face, a negative fluid pressure exerts an inward pressure *P* normal to the face, and its four adjacent faces exert two pairs of forces its four edges, as shown in Figure 1A ii. Each pair of forces can be divided into a normal component, which produces bending deformation coupled with *P*, and a tangential component, which produces compressive deformation.

As shown in Figure 1A iii, a crease structure on a side face results in the smallest bending stiffness in the direction perpendicular to its crease line in its adjacent area, so the side face tends to bend in the direction perpendicular to the crease lines when a negative fluid pressure is applied. The crease structures also bring a local stiffness difference at each side edge, which makes it incline when actuated, as shown in Figure 1A iv. Taking a TCC as an example, the largest bending deformation occurs in the direction perpendicular to the slanted crease line on the diagonal of each side face. All four side edges incline in the same direction and then collapse along the inclined direction, leading to the subsequent folding motion of twisting and

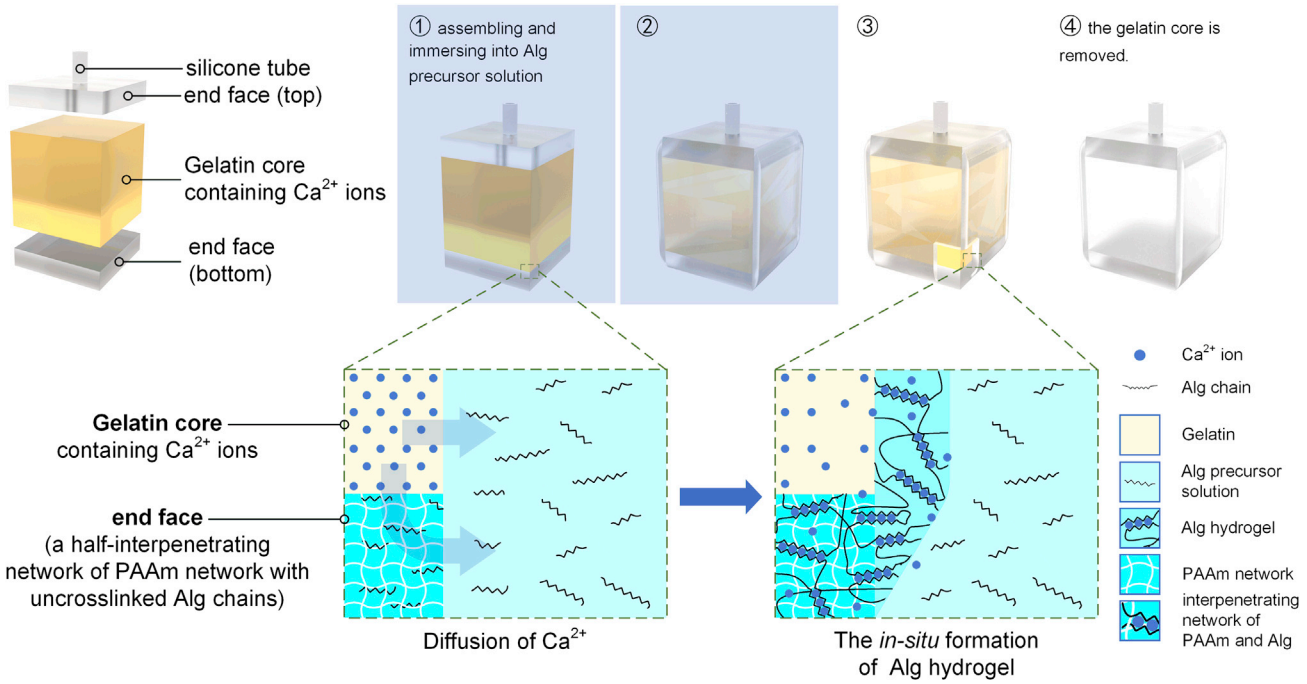

Figure 2. Schematic illustration of the fabrication process of a CAU

A solid gelatin core with a predesigned crease pattern and containing calcium ions (Ca^{2+}) is immersed into a sodium alginate (Alg) precursor solution. Then, Ca^{2+} ions begin to diffuse inside-out and induce the ionic crosslinking of Alg chains, resulting in the *in situ* formation of a thin-walled Alg hydrogel shell on the surface of the core. Finally, the core is removed, and A CAU with 3D thin-walled hollow hydrogel structure is obtained.

contraction. In addition, a crease structure of the valley or mountain line guides its folding direction and the plastic predeformation at the creases after folding further reduces the bending stiffness in the direction perpendicular to the crease lines and ensures the subsequent folding movements. As a result, if the crease structures are added on each side face, they would divide each side face into multiple facets, and the facets would fold along the crease lines when a negative fluid pressure is applied.

Fabrication of CAUs

In nature, arthropods grow and molt their thin-walled exoskeletons on the outside surfaces of their bodies. Inspired by this, a facile fabrication strategy based on removable templates and inside-out ion-diffusion-induced *in situ* crosslinking was used to fabricate CAUs with 3D thin-walled hollow hydrogel structures. Specifically, steps of the fabrication strategy are shown in Figure 2. First, a solid gelatin core containing calcium ions (Ca^{2+}) can simply be molded to form its shape with a predesigned crease pattern. Two end faces are molded by covalently crosslinking a PAAm network, which forms a half-interpenetrating network of the PAAm network with uncrosslinked Alg chains. A silicone fluidic connector is also attached on the top face during the molding process by covalent grafting of the PAAm network with the silicone surface (Yuk et al., 2017). Then, the two end faces are assembled on the gelatin core and the assembly is completely immersed into a sodium alginate (Alg) precursor solution, and Ca^{2+} ions begin to diffuse inside-out and induce the ionic crosslinking of Alg chains, resulting in the *in situ* formation of a thin-walled Alg hydrogel shell on the surface of the core. During this process, part of the uncrosslinked Alg chains in the two end faces is also physically crosslinked and connects the two end faces to the formed thin-walled Alg hydrogel shell by an PAAm-Alg interpenetrating network. Finally, the core is melted and removed in hot water, and A CAU with a 3D thin-walled hollow hydrogel structure is obtained.

A simplified planar hydrogel *in situ* forming model (2D), as shown in Figure 3A, was used to investigate the forming process. As shown in Figure 3B, a uniform Alg hydrogel layer formed *in situ* on the top surface of a gelatin layer. As shown by the SEM image in Figure 3C, the two layers were clearly divided, where the Alg

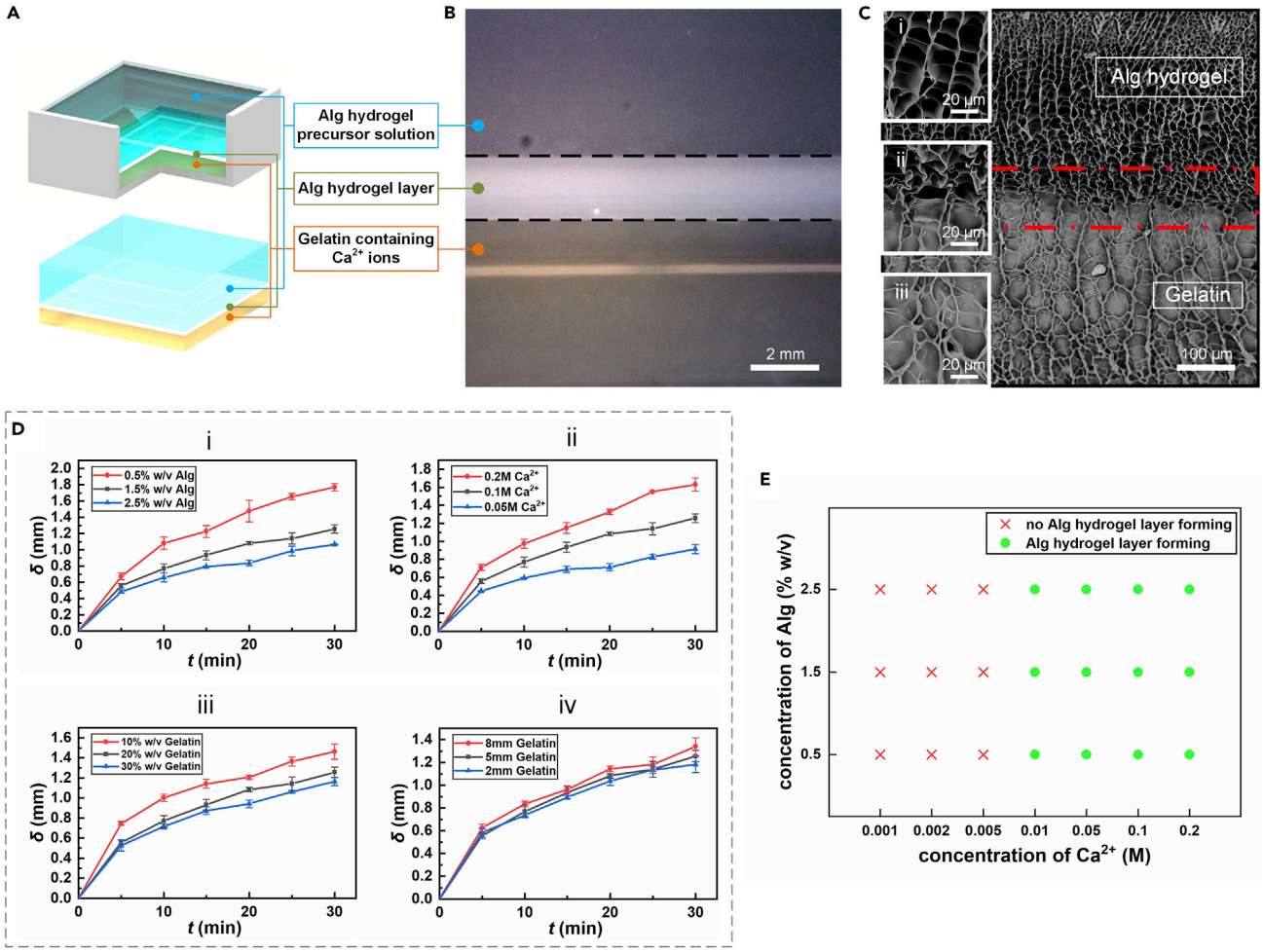

Figure 3. "Hydrogel *in situ* forming" process investigated by a simplified planar model

(A) Schematic of the 2D "hydrogel *in situ* forming" model: A simplified planar hydrogel *in situ* forming model (2D) was used to investigate the forming process.

(B) A cross-section image of the Alg hydrogel forming process: A uniform Alg hydrogel layer formed *in situ* on the top surface of a gelatin layer. (Scale bar = 2 mm).

(C) A SEM image showing the microscopic morphology of the *in-situ*-formed Alg hydrogel: The Alg hydrogel layer and the gelatin layer were clearly divided. (Scale bar = 100 and 20 μm).

(D) Thickness-time curves for regulating the thickness of the *in-situ*-formed Alg hydrogel layers: The Alg hydrogel layers thicken over time at different forming rates, influenced by the concentration of Alg precursor solution, the concentration of Ca^{2+} and gelatin in the gelatin layer, and the thickness of the gelation layer. See also Table S1. (Data are represented as mean ± SD).

(E) The concentration of Ca^{2+} for hydrogel gelation: Alg hydrogel layers formed or not after a sufficient formation time (8 h herein) with different concentrations of Ca^{2+} and Alg.

hydrogel layer had an open-pore microstructure, while the gelatin layer had a denser closed-pore microstructure.

Figures 3D i–iv show the thickness (δ) of the Alg hydrogel layer as it formed over time. Four impact factors were investigated, including the concentration of Alg precursor solution, the concentrations of Ca^{2+} and gelatin in the gelatin layer, and the thickness of the gelation layer. The experimental results show that the formation rate of the Alg hydrogel layer increases significantly as the concentration of Ca^{2+} increases. The increase in the concentrations of Alg and gelatin obviously slows the formation of Alg hydrogel layers, because the increasing viscosity of precursor solution and density of the gelation layer hinder the diffusion of Ca^{2+} ions. Else, the thickness of the gelatin layer, which affects the surface-volume ratio, had a relatively small effect herein. This indicates that in the early period of the Alg hydrogel formation process, its

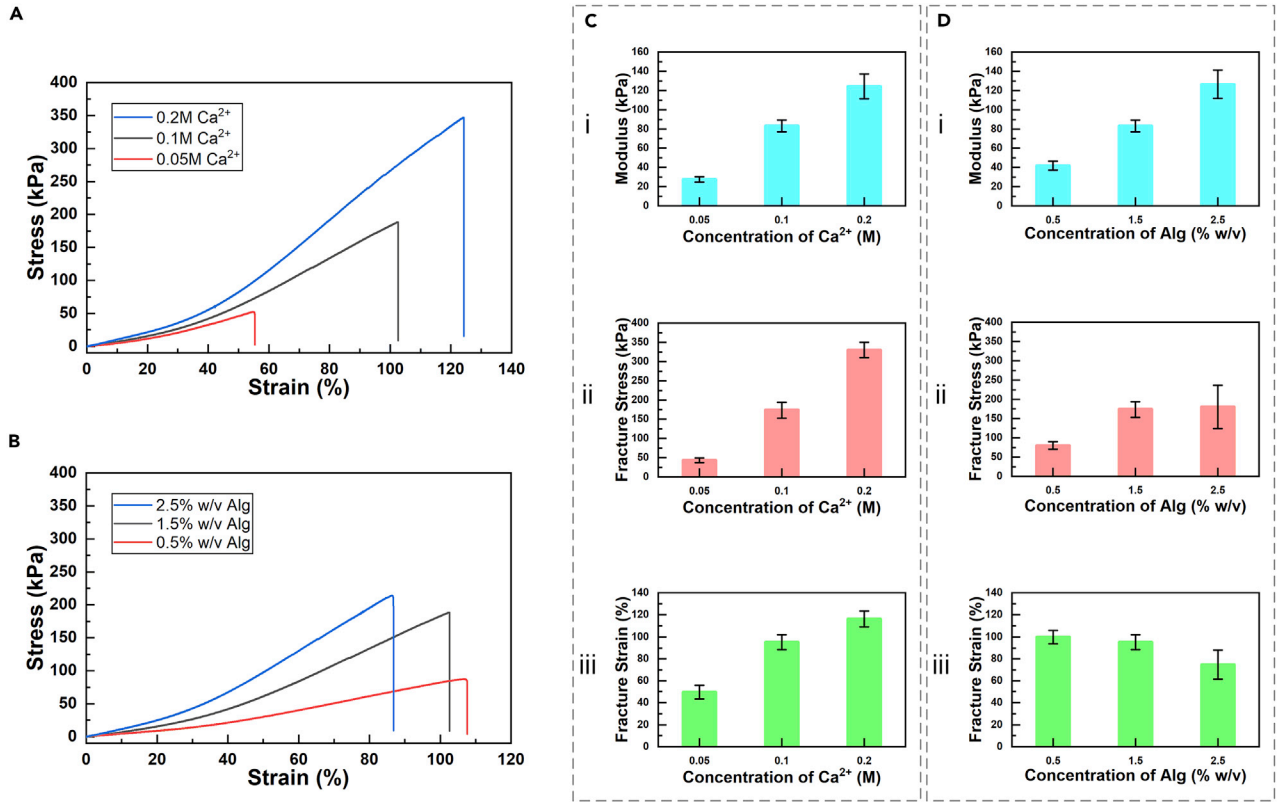

Figure 4. Tensile tests for the mechanical data of the formed Alg hydrogel layers

(A and C) Stress-strain curves and the mechanical data of Alg hydrogel layers formed with different concentrations of Ca^{2+}. (Data are represented as mean ± SD).

(B and D) Stress-strain curves and the mechanical data of hydrogel layers formed with different concentrations of Alg. (Data are represented as mean ± SD). See also Figure S1.

crosslinking is mainly induced by Ca^{2+} ions on the surface of the gelatin layer, and the supplementation of Ca^{2+} ions from the bottom of the gelatin layer is not obvious, which may be due to the slow diffusion of Ca^{2+} ions in the dense gelatin layer. In addition, Figure 3E shows whether Alg hydrogel layers form on the surface of gelatin layers after a sufficient formation time (8 h herein) with different concentrations of Ca^{2+} and Alg. It can be considered that the concentration of Ca^{2+} is the major factor, and Alg hydrogel layers cannot form when it is less than 0.01 M.

Tensile tests were conducted to obtain the mechanical data of the Alg hydrogel layers formed with different concentrations of Ca^{2+} and Alg. From the stress-strain curves shown in Figures 4A and 4B, the tensile moduli, fracture strain, and fracture stress can be obtained, as shown in Figures 4C and 4D. The tensile modulus and fracture stress increase with increasing concentrations of Ca^{2+} and Alg, possibly because of the increasing density of ionic bonds and Alg chains. The fracture strain increases as the concentrations of Ca^{2+} increases, which may be because of the increasing density of ionic bonds, while it decreases as the concentration of Alg increases, which may be because of the decrease in material uniformity due to the longer forming time.

Actuation tests of CAUs

CAUs can be actuated continuously, which are controlled by the volume change of the driving fluids. The actuation performances of the CAUs were tested and their actuation processes are shown in Figure 5. The actuation processes were tested at a volume change rate of 3 mL/min.

LCCs performed a linear contraction motion to its maximum length change of contraction (ΔH) of appr. 6.431 mm, with a maximum relative length change of contraction ($\Delta H/H$) of appr. 47.580%. TBCs performed

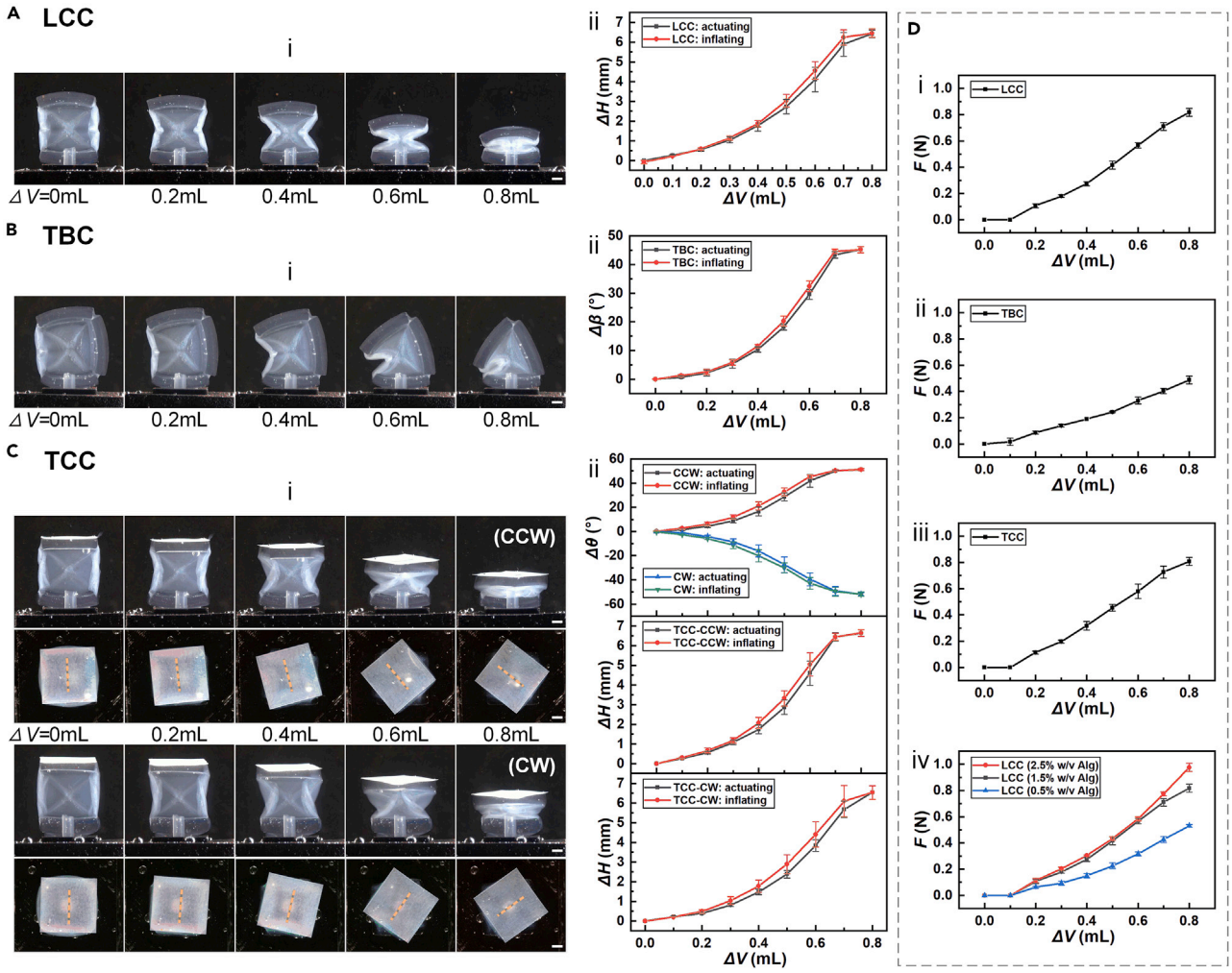

Figure 5. Actuation tests of CAUs

(A–C) Actuation processes and actuation curves of LCC, TBC, and TCC-CCW/CW, respectively: CAUs were actuated continuously, controlled by the volume change of the driving fluids. See also Videos S1, S2 and S3. (Scale bar = 2 mm; Data are represented as mean ± SD).

(D) Output forces curves of CAUs as volume changes: The output forces increased with the increase of negative fluid pressure caused by volume change. (Data are represented as mean ± SD. See also Figure S3).

a tilting motion with a maximum angle change of tilting ($\Delta\beta$) of appr. 45.182°. TCCs performed a coupled motion of twisting and contraction, with a maximum angle change of twisting ($\Delta\theta$) of appr. 51.092° (CCW) and 51.845° (CW) and a maximum length change of contraction (ΔH) of appr. 6.639 mm (CCW) and 6.532 mm (CW) ($\Delta H/H$ = 54.258% (CCW) and 50.810% (CCW)). The actuation processes of the tested TCC-CCW and TCC-CW were nearly symmetrical, as designed. In addition, their actuation speed can be controlled by the volume change rate of the driving fluids, for examples, the CAUs completed a single actuation stroke in appr. 4s when the volume of their driving fluids change at 12 mL/min (as shown in Videos S1, S2 and S3).

The output forces of CAUs as volume changes were also tested. The output forces increased with the increase of negative fluid pressure caused by volume change. In addition, from the output force curves of LCCs fabricated with different concentrations of Alg, the LCCs made from higher concentration of Alg, which results in larger tensile moduli in their Alg hydrogel layers, have larger output forces.

However, high concentration of Alg precursor solution results in poor fluidity that increases the fabricating difficulty of preparing small structures and removing residual precursor solution, while high concentration

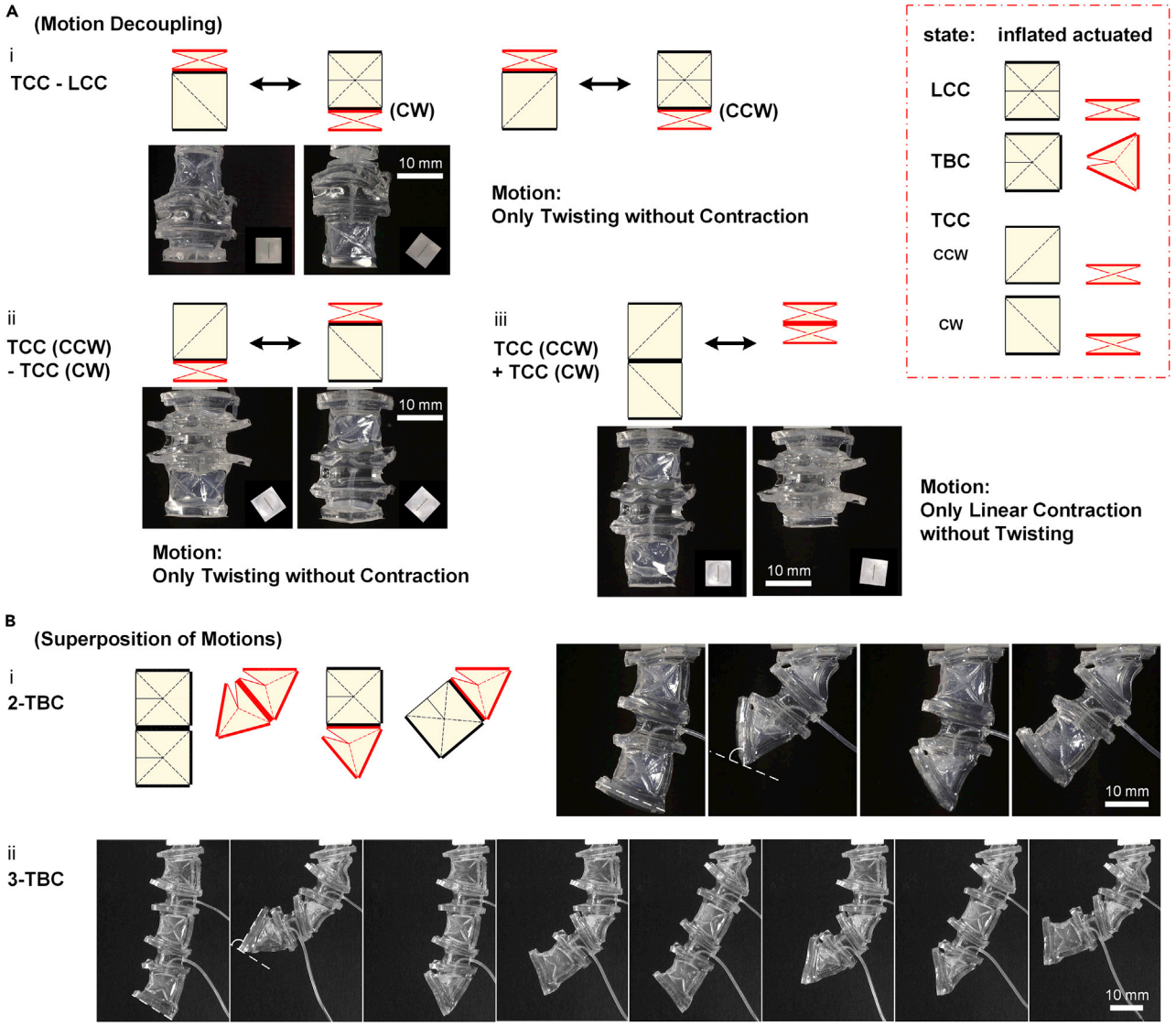

Figure 6. Combinations of CAUs

(A) Actuation decoupling: A combination of a TCC and an LCC achieved an approximate single twisting motion through the coordination of their actuation states. Likewise, a combination of a TCC-CCW and a TCC-CW achieved an approximate single twisting motion or an approximate single linear motion (elongation & contraction). See also Video S4. (Scale bar = 10 mm).

(B) Actuation superposition: The combinations of multiple TBCs achieved a superimposed angle change of bending. See also Video S5. (Scale bar = 10 mm).

of Ca^{2+} results in a rapid formation rate that reduces the operability of the fabrication processes. Tradeoffs of actuation performance, preparation time, and manufacturability, herein, the tested CAUs and the application demos as demonstrations were prepared with a moderate concentration of Alg (1.5% w/v) and Ca^{2+} (0.1 M).

Combinations of CAUs

In nature, biological actuation systems achieve more complex and flexible actuation through combinations of multiple actuation units. With the modular design of CAUs, different combinations of multiple CAUs were used to achieve different actuation modes and reprogramming of shape changes.

Combinations of multiple CAUs can realize motion decoupling. As shown in Figures 6A, combination of one TCC and one LCC achieved an approximate single twisting motion through the coordination of their

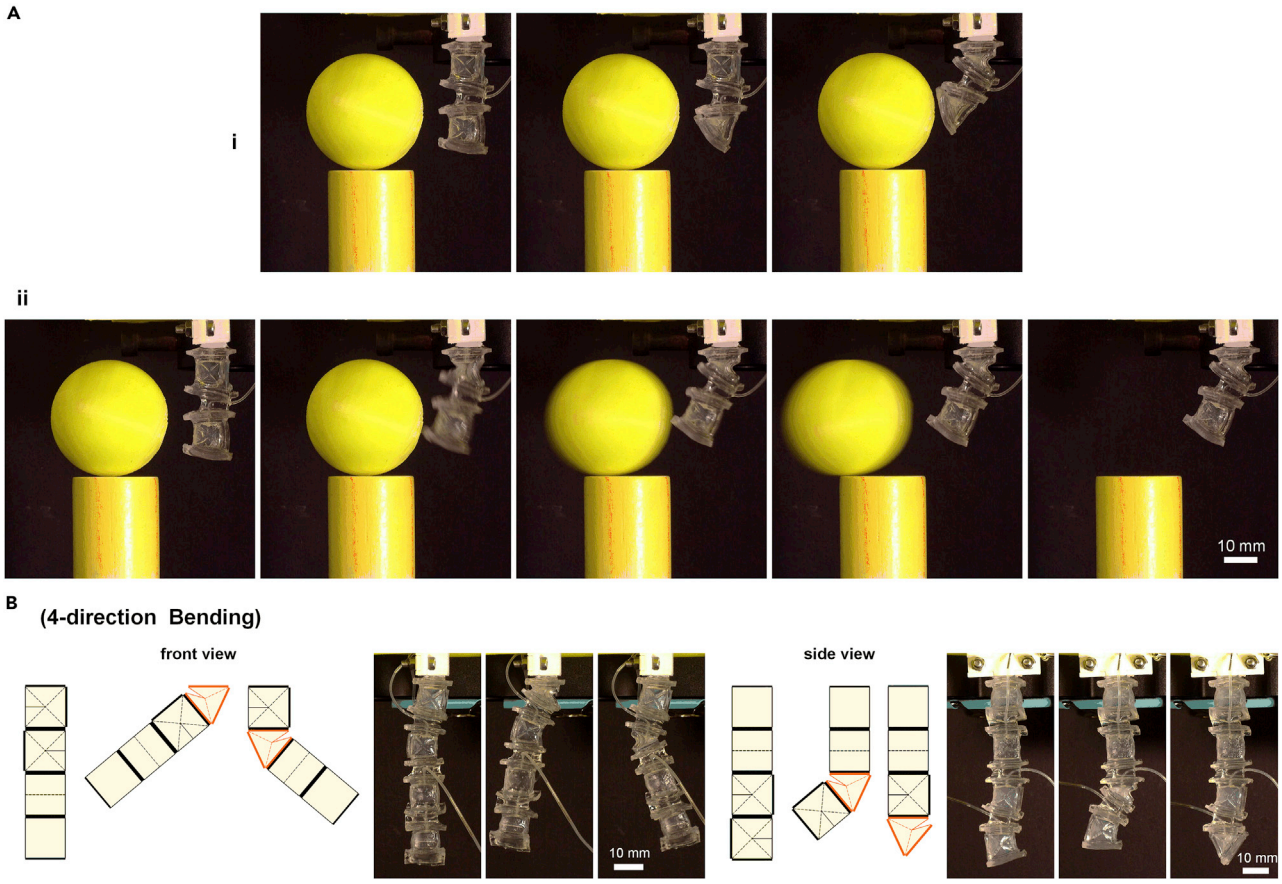

Figure 7. Reprogramming of actuation modes and shape changes

(A) Two different actuation sequences of a 2-TBC finger-like bending actuator determined whether a ball can be kicked. See also Video S6. (Scale bar = 10 mm).

(B) On-demand actuation of a multiple-TBC actuator achieved a 4-direction bending motions. (Scale bar = 10 mm).

actuation states. Likewise, a combination of one TCC-CCW and one TCC-CW achieved an approximate single twisting motion or an approximate linear elongation & contraction motion through two different modes of actuation (as shown in Video S4).

Combinations of multiple CAUs can also realize actuation superposition. As shown in Figure 6B and Video S5, a 2-TBC bending actuator, the combination of two TBCs, achieved a superimposed angle change of bending, whose maximum were appr. 66°. In the same way, a 3-TBC bending actuator achieved a maximum angle change of bending of appr. 88°. In addition, the independent actuation of each single CAU enables the sequential actuation of their combination. (Videos S4 and S5).

What's more, combinations of multiple CAUs enable reprogramming of actuation modes and shape changes. As shown in Figure 7A and Video S6, two different actuation sequences of a 2-TBC finger-like bending actuator determine whether a ball can be kicked. As shown in Figure 7B, a tentacle, consisting of four TBCs that arranged in different directions, achieved a 4-direction bending motion through on-demand actuation.

Application demos for different tasks

As shown in Figure 8, herein, a two-finger gripper and a three-finger gripper were demonstrated as simple application demos for grasping applications. The two-finger gripper, consisting of two LCCs, was capable of picking and placing an object, such as a weight-shaped object (which weighs 7.790 g, as shown in Figures 8A i, ii and Video S7). What's more, benefiting from the controllable actuation of CAUs, objects of different widths (which are 1, 2, 4, 6, 8, 12, 14, and 16 mm wide, respectively, as shown in Figure 8A iii) can be grasped successfully. As

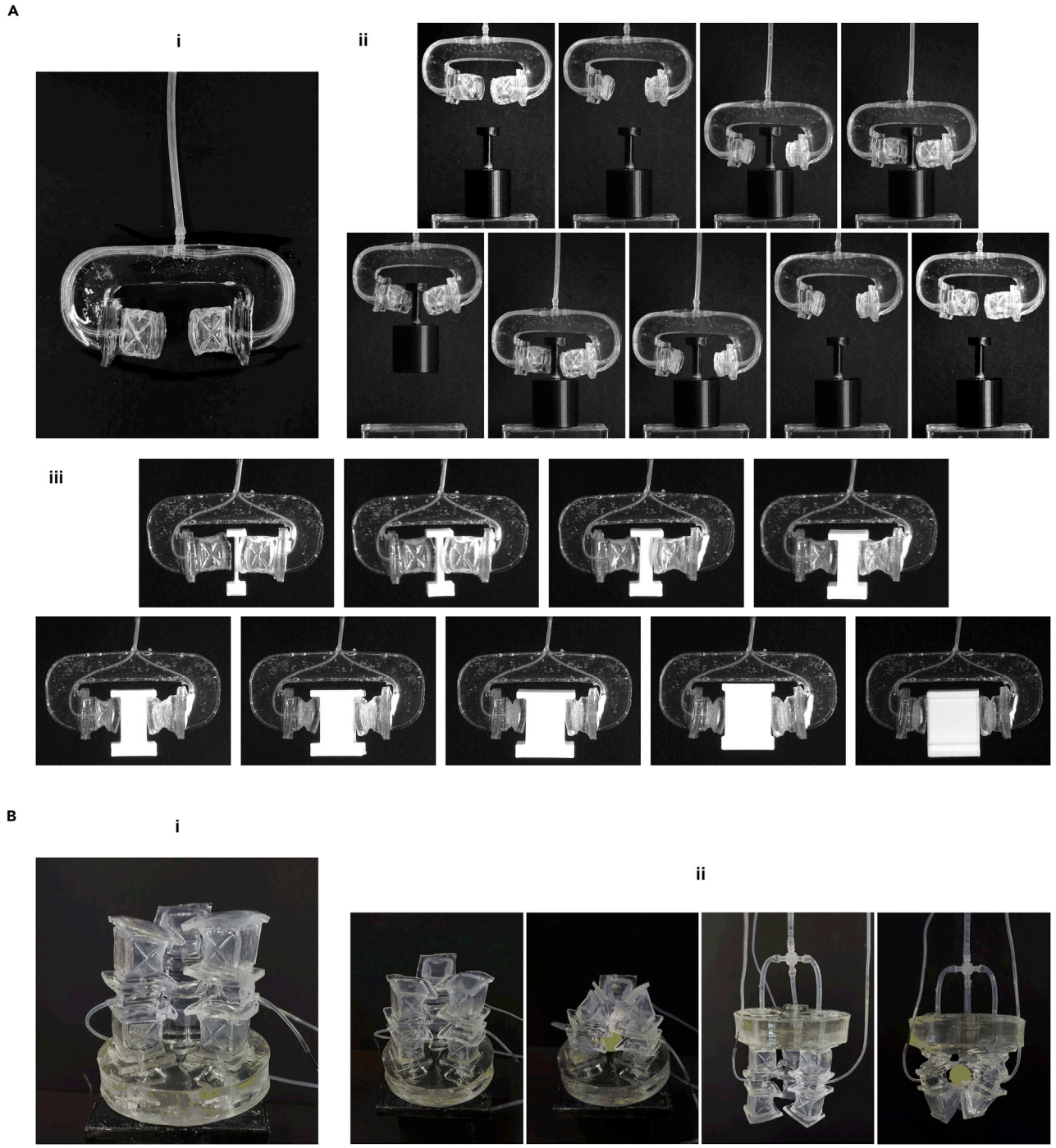

Figure 8. Simple application demos for grasping tasks

(A) A two-finger gripper: The two-finger gripper, consisting of two LCCs, was capable of picking and placing an object. Benefiting from the controllable actuation of CAUs, objects of different widths (which are 1, 2, 4, 6, 8, 12, 14, and 16 mm wide, respectively) can be grasped successfully. See also Video S7.

(B) A three-finger gripper: The three-finger gripper, consisting of multiple TBCs, can hold and release an object like a hand. See also Video S8.

shown in Figure 8B and Video S8, the three-finger gripper, consisting of multiple TBCs, can hold and release an object like a hand, such as a spherical object. Moreover, as shown in Figure 9 and Video S9, a TCC-CCW, a TCC-CW, and an LCC were combined onto a two-finger gripper, which was capable of picking up a coin and inserting it into a slot at a particular angle (90° relative to its original position herein). This demonstrated the potential of

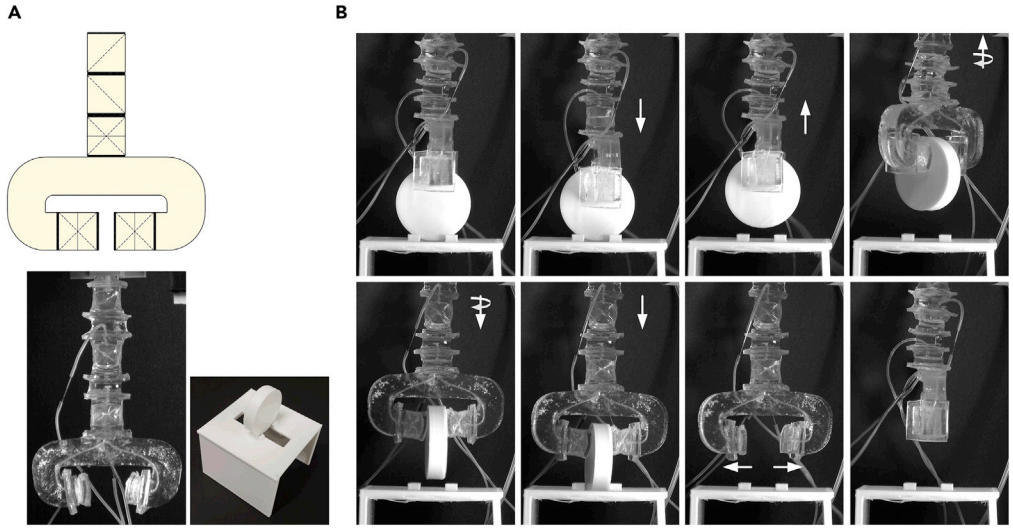

Figure 9. A two-finger gripper with twisting ability, performing a task of coin inserting

(A) A TCC-CCW, a TCC-CW, and an LCC were combined onto a two-finger gripper.

(B) It was capable of picking up a coin and inserting it into a slot at a particular angle (90° relative to its original position herein). See also.

the fluid-driven hydrogel actuators with origami structures herein for further application in grasping tasks, performing functions like fingers and wrists of human.

What's more, as shown in Figure 10 and Video S10, a combination of a TCC-CCW, a TCC-CW, and an LCC, with a strip of electrically conductive copper film attached to its bottom face, was used as a multi-way switch of an electric circuit. With the controllable actuation of CAUs, it was capable of aligning the copper strip with pins of different circuits distributed in both directions through the angle changes of the two TCCs, and adjusting the height of the copper strip to control the corresponding circuit on and off by the LCC. As a demonstration, herein, it controlled the on and off states of lights of three different colors: yellow (0°), green (22.5°), and red (−22.5°).

DISCUSSION

The introduction of origami structures to the design of fluid-driven hydrogel actuators has achieved diverse actuation movements, including linear motion (elongation & contraction), twisting, and bending, whose actuation states and actuation speeds can be simply controlled by the driving fluids. Owing to the configuration of crease structures, the cuboid hydrogel actuators tend to bend in the direction perpendicular to the crease lines when driven by a negative fluid pressure. This guides them to fold directionally according to the predesigned crease patterns and produce different types of actuation movements.

Compared with the existing fluid-driven hydrogel actuators (Yuk et al., 2017; Shintake et al., 2017; Zhang et al., 2018; Mishra et al., 2020; Takishima et al., 2021; Mishra et al., 2021; Hardman et al., 2022), whose practical applications would be restricted by their lack of actuation diversity, the fluid-driven hydrogel actuators with origami structures herein achieve more diverse actuation movements through different origami designs. With the modular design thinking, combinations of multiple actuator modules can realize actuation combinations and reprogramming of actuation modes. The superposition of CAUs can realize the increase of the maximum actuation, demonstrating that the modular design enables extensibility of actuation ability to CAUs, although due to the gravity and the restriction of the end faces, the maximum actuation cannot reach the sum of the maximum actuation of CAUs of equal number. The maximum actuation of multi-CAU combinations would be larger when they actuate in the horizontal plane or in water. Moreover, the design methodology of origami structures for fluid-driven hydrogel actuators is scalable and has the potential to be extended more complex origami design.

A facile fabrication strategy has been adopted for 3D thin-walled hollow hydrogel actuators with origami structures herein. Compared with molding methods (Shintake et al., 2017; Yuk et al., 2017; Zhang et al., 2018;

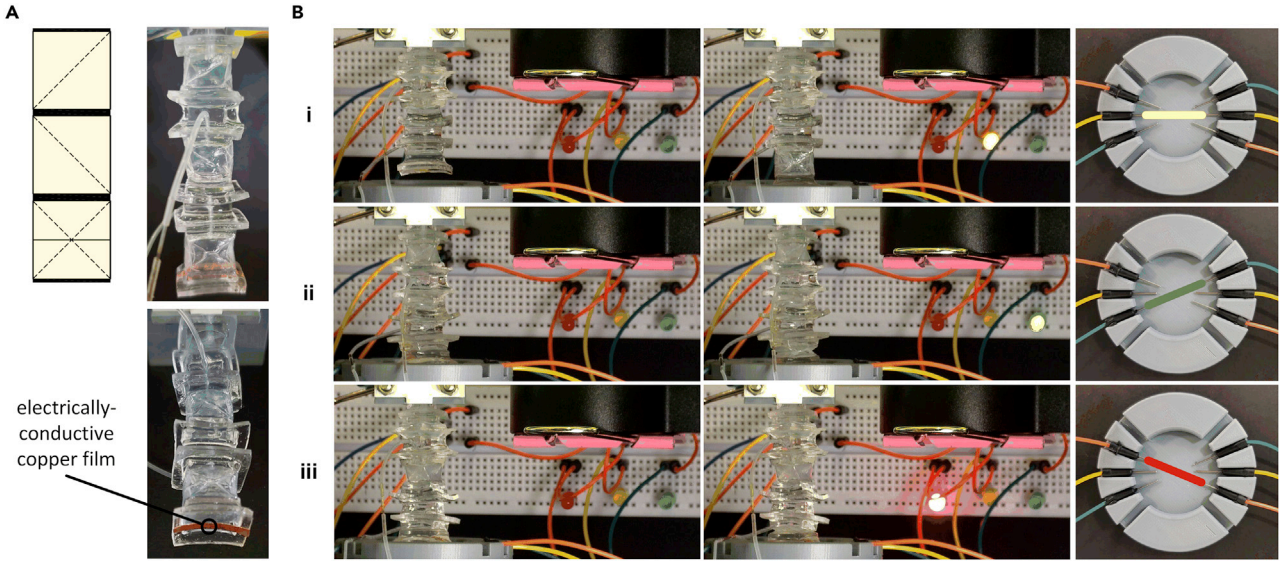

Figure 10. A multi-way circuit switch, controlling three lights of different colors on and off

(A) A combination of a TCC-CCW, a TCC-CW, and an LCC, with a strip of electrically conductive copper film attached to its bottom face, was used as a multi-way electric switch.

(B) Herein, it controlled the on and off states of lights of three colors as a demonstration. See also.

Hardman et al., 2022), this facile fabrication strategy is capable of fabricating 3D thin-walled hollow hydrogels with complex shapes and structures. Unlike 3D printing methods for hydrogels (including direct-ink-write (Cheng et al., 2019; Heiden et al., 2022) and stereolithography (Mishra et al., 2020; Mishra et al., 2021; Takishima et al., 2021)), its equipment is readily available and low cost. The thickness and mechanical properties of the formed thin-walled hydrogels can be regulated by adjusting the forming time and the processes of ion diffusion and hydrogel crosslinking, including the concentration of the precursor solution, the concentration of initiators, properties of template materials, shape of templates, and so on. Moreover, the fabrication strategy has the potential to be extended to other ionic crosslinked hydrogels (Ma et al., 2018a; Ma et al., 2018b; Lin et al., 2019; Zhou et al., 2020), and even other initiator-induced chemical crosslinked polymers (Yu et al., 2019; Subraveti and Raghavan, 2021). This is of significance, as it can possibly be adopted with new hydrogel materials with better properties to further enhance the performance of actuators. Furthermore, the combination of multiple materials would further enable more innovative functions, and the applications of the fluid-driven hydrogel actuators with origami structures herein are expected to be further explored.

However, the mechanism of ion diffusion and hydrogel crosslinking can be further investigated for templates with complex 3D shapes, and a numerical simulation model based on hydrogel materials and fluid actuation can be further built for CAUs design and fabrication optimization for different applications through structural and material optimization, as well as for designing more complex origami structures for different tasks.

In summary, aiming at the diverse actuation functionality for fluid-driven hydrogel actuators, a new structural design methodology based on origami structures was proposed and a facile fabrication strategy based on removable templates and inside-out diffusion-induced *in situ* crosslinking was adopted for constructing 3D thin-walled hollow hydrogel structures. This would give hydrogel soft actuators new possibilities to endow innovative functions for biomimetic soft robotics in research or engineering fields. Although herein they are still a concept, the fluid-driven hydrogel actuators with origami structures are expected to be used in practical applications, such as underwater and surgical tasks, in the future.

Conclusion

This paper proposes a novel type of fluid-driven hydrogel actuator with origami structures and a facile fabrication strategy based on removable templates and inside-out diffusion-induced crosslinking. The fabrication process was investigated, where the thickness and mechanical properties of the formed hydrogels

could be regulated by adjusting the ion diffusion process and the forming time. As a result, three basic types of modular actuator units of linear motion, bending, and twisting were fabricated and their actuation performances were tested. It demonstrates the feasibility and extensibility of origami structures for the actuation diversity of fluid-driven hydrogel actuators. Moreover, multiple CAUs were combined to achieve decoupling, superposition, and reprogramming of actuation. In addition, several simple application demos of multiple-finger grippers and a multi-way circuit switch further demonstrated their potential for further applications.

Limitations of the study

First, the shape and actuation of the CAU prototypes fabricated and tested in this paper have relatively large variances due to manufacturing errors from their hand-made processes. Second, the mechanism of ion diffusion and hydrogel crosslinking should be further investigated to better regulate the thickness and mechanical properties of the formed thin-walled hollow hydrogels with complex 3D shapes. Third, a numerical simulation model based on hydrogel materials and fluid actuation should be further built for CAUs design and fabrication optimization, as well as for more complex origami design for different tasks. Additionally, more practical applications need to be explored in the future.

STAR★METHODS

Detailed methods are provided in the online version of this paper and include the following:

- KEY RESOURCES TABLE
- RESOURCE AVAILABILITY
  - Lead contact
  - Materials availability
  - Data and code availability
- METHOD DETAILS
  - Materials
  - Characterization of the ''hydrogel in situ forming'' process
  - Fabrication of CAUs
  - Actuation test of CAUs
  - Combinations of CAUs and fabrication of application demos
- QUANTIFICATION AND STATISTICAL ANALYSIS

SUPPLEMENTAL INFORMATION

Supplemental information can be found online at https://doi.org/10.1016/j.isci.2022.104674.

ACKNOWLEDGMENTS

The authors acknowledge financial support from the Project of Basic Research of Shenzhen, China (JCYJ20180507183655307).

AUTHOR CONTRIBUTIONS

Conceptualization, Z.H.; Methodology, Z.H. and Z.G.; Investigation, Z.H. and C.W.; Writing—Original Draft, Z.H.; Writing—Review & Editing, S.M., Z.G., C.W., L.D., A.W., and H.Y.; Supervision, S.M.; Project Administration, Z.H. and Z.G.; Funding Acquisition, S.M.

DECLARATION OF INTERESTS

The authors declare no competing interests.

Received: May 3, 2022
Revised: June 3, 2022
Accepted: June 21, 2022
Published: July 15, 2022

REFERENCES

Banerjee, H., Suhail, M., and Ren, H. (2018). Hydrogel actuators and sensors for biomedical soft robots: brief overview with impending challenges. Biomimetics *3*, 15. https://doi.org/10.3390/biomimetics3030015.

Baumgartner, M., Hartmann, F., Drack, M., Preninger, D., Wirthl, D., Gerstmayr, R., Lehner, L., Mao, G., Pruckner, R., Demchyshyn, S., et al. (2020). Resilient yet entirely degradable gelatin-based biogels for soft robots and electronics. Nat. Mater. *19*, 1102–1109. https://doi.org/10.1038/s41563-020-0699-3.

Cheng, Y., Chan, K.H., Wang, X.Q., Ding, T., Li, T., Lu, X., and Ho, G.W. (2019). Direct-ink-write 3D printing of hydrogels into biomimetic soft robots. ACS Nano *13*, 13176–13184. https://doi.org/10.1021/acsnano.9b06144.

Coyle, S., Majidi, C., LeDuc, P., and Hsia, K.J. (2018). Bio-inspired soft robotics: material selection, actuation, and design. Extreme Mech. Lett. *22*, 51–59. https://doi.org/10.1016/j.eml.2018.05.003.

D'eramo, L., Chollet, B., Leman, M., Martwong, E., Li, M., Geisler, H., Dupire, J., Kerdraon, M., Vergne, C., Monti, F., et al. (2018). Microfluidic actuators based on temperature-responsive hydrogels. Microsyst. Nanoeng. *4*, 17069. https://doi.org/10.1038/micronano.2017.69.

Ding, M., Jing, L., Yang, H., Machnicki, C.E., Fu, X., Li, K., Wong, I.Y., and Chen, P.Y. (2020). Multifunctional soft machines based on stimuli-responsive hydrogels: from freestanding hydrogels to smart integrated systems. Mater. Today Adv. *8*, 100088. https://doi.org/10.1016/j.mtadv.2020.100088.

Downs, F.G., Lunn, D.J., Booth, M.J., Sauer, J.B., Ramsay, W.J., Klemperer, R.G., Hawker, C.J., and Bayley, H. (2020). Multi-responsive hydrogel structures from patterned droplet networks. Nat. Chem. *12*, 363–371. https://doi.org/10.1038/s41557-020-0444-1.

Duan, J., Liang, X., Zhu, K., Guo, J., and Zhang, L. (2017). Bilayer hydrogel actuators with tight interfacial adhesion fully constructed from natural polysaccharides. Soft Matter *13*, 345–354. https://doi.org/10.1039/C6SM02089E.

Göttler, C., Elflein, K., Siegwart, R., and Sitti, M. (2021). Spider origami: folding principle of jumping spider leg joints for bioinspired fluidic actuators. Adv. Sci. *8*, 2003890. https://doi.org/10.1002/advs.202003890.

Han, D., Farino, C., Yang, C., Scott, T., Browe, D., Choi, W., Freeman, J.W., and Lee, H. (2018). Soft robotic manipulation and locomotion with a 3D printed electroactive hydrogel. ACS Appl. Mater. Interfaces *10*, 17512–17518. https://doi.org/10.1021/acsami.8b04250.

Hardman, D., George Thuruthel, T., and Iida, F. (2022). Self-healing ionic gelatin/glycerol hydrogels for strain sensing applications. NPG Asia Mater. *14*, 11. https://doi.org/10.1038/s41427-022-00357-9.

Heiden, A., Preninger, D., Lehner, L., Baumgartner, M., Drack, M., Woritzka, E., Schiller, D., Gerstmayr, R., Hartmann, F., and Kaltenbrunner, M. (2022). 3D printing of resilient biogels for omnidirectional and exteroceptive soft actuators. Sci. Robot. *7*, eabk2119. https://doi.org/10.1126/scirobotics.abk2119.

Ilami, M., Bagheri, H., Ahmed, R., Skowronek, E.O., and Marvi, H. (2021). Materials, actuators, and sensors for soft bioinspired robots. Adv. Mater. *33*, 2003139. https://doi.org/10.1002/adma.202003139.

Ionov, L. (2014). Hydrogel-based actuators: possibilities and limitations. Mater. Today *17*, 494–503. https://doi.org/10.1016/j.mattod.2014.07.002.

Jiao, D., Zhu, Q.L., Li, C.Y., Zheng, Q., and Wu, Z.L. (2022). Programmable morphing hydrogels for soft actuators and robots: from structure designs to active functions. Acc. Chem. Res. *55*, 1533–1545. https://doi.org/10.1021/acs.accounts.2c00046.

Jiao, Z., Zhang, C., Ruan, J., Tang, W., Lin, Y., Zhu, P., Wang, J., Wang, W., Yang, H., and Zou, J. (2021). Re-foldable origami-inspired bidirectional twisting of artificial muscles reproduces biological motion. Cell Rep. Phys. Sci. *2*, 100407. https://doi.org/10.1016/j.xcrp.2021.100407.

Kim, W., Byun, J., Kim, J.K., Choi, W.Y., Jakobsen, K., Jakobsen, J., Lee, D.Y., and Cho, K.J. (2019). Bioinspired dual-morphing stretchable origami. Sci. Robot. *4*, eaay3493. https://doi.org/10.1126/scirobotics.aay3493.

Le, X., Lu, W., Zhang, J., and Chen, T. (2019). Recent progress in biomimetic anisotropic hydrogel actuators. Adv. Sci. *6*, 1801584. https://doi.org/10.1002/advs.201801584.

Lee, J.G., and Rodrigue, H. (2019). Origami-based vacuum pneumatic artificial muscles with large contraction ratios. Soft Robot. *6*, 109–117. https://doi.org/10.1089/soro.2018.0063.

Lee, Y., Song, W.J., and Sun, J.Y. (2020). Hydrogel soft robotics. Mater. Today Phys. *15*, 100258. https://doi.org/10.1016/j.mtphys.2020.100258.

Li, C., Lau, G.C., Yuan, H., Aggarwal, A., Dominguez, V.L., Liu, S., Sai, H., Palmer, L.C., Sather, N.A., Pearson, T.J., Freedman, D.E., Amiri, P.K., de la Cruz, M.O., and Stupp, S.I. (2020). Fast and programmable locomotion of hydrogel-metal hybrids under light and magnetic fields. Sci. Robot. *5*, eabb9822. https://doi.org/10.1126/scirobotics.abb9822.

Li, S., Stampfli, J.J., Xu, H.J., Malkin, E., Diaz, E.V., Rus, D., and Wood, R.J. (2019). A vacuum-driven origami " magic-ball " soft gripper. In International Conference on Robotics & Automation, pp. 7401–7408.

Li, S., Vogt, D.M., Rus, D., and Wood, R.J. (2017). Fluid-driven origami-inspired artificial muscles. Proc. Natl. Acad. Sci. U S A. *114*, 13132–13137. https://doi.org/10.1073/pnas.1713450114.

Lin, H., Ma, S., Yu, B., Cai, M., Zheng, Z., Zhou, F., and Liu, W. (2019). Fabrication of asymmetric tubular hydrogels through polymerization-assisted welding for thermal flow actuated artificial muscles. Chem. Mater. *31*, 4469–4478. https://doi.org/10.1021/acs.chemmater.9b00965.

Lin, Y., Yang, G., Liang, Y., Zhang, C., Qian, D., Yang, H., and Zou, J. (2020). Controllable stiffness origami " skeletons " for lightweight and multifunctional artificial muscles. Adv. Funct. Mater. *30*, 2000349. https://doi.org/10.1002/adfm.202000349.

Liu, X., Liu, J., Lin, S., and Zhao, X. (2020). Hydrogel machines. Mater. Today *36*, 102–124. https://doi.org/10.1016/j.mattod.2019.12.026.

Ma, S., Rong, M., Lin, P., Bao, M., Xie, J., Wang, X., Huck, W.T.S., Zhou, F., and Liu, W. (2018a). Fabrication of 3D tubular hydrogel materials through on-site surface free radical polymerization. Chem. Mater. *30*, 6756–6768. https://doi.org/10.1021/acs.chemmater.8b02532.

Ma, S., Yan, C., Cai, M., Yang, J., Wang, X., Zhou, F., and Liu, W. (2018b). Continuous surface polymerization via Fe(II)-Mediated redox reaction for thick hydrogel coatings on versatile substrates. Adv. Mater. *30*, e1803371. https://doi.org/10.1002/adma.201803371.

Mishra, A.K., Pan, W., Giannelis, E.P., Shepherd, R.F., and Wallin, T.J. (2021). Making bioinspired 3D-printed autonomic perspiring hydrogel actuators. Nat. Protoc. *16*, 2068–2087. https://doi.org/10.1038/s41596-020-00484-z.

Mishra, A.K., Wallin, T.J., Pan, W., Xu, P., Wang, K., Giannelis, E.P., Mazzolai, B., and Shepherd, R.F. (2020). Autonomic perspiration in 3D-printed hydrogel actuators. Sci. Robot. *5*, 1–10. https://doi.org/10.1126/scirobotics.aaz3918.

Park, N., and Kim, J. (2020). Hydrogel-based artificial muscles: overview and recent progress. Adv. Intell. Syst. *2*, 1900135. https://doi.org/10.1002/aisy.201900135.

Shang, J., Le, X., Zhang, J., Chen, T., and Theato, P. (2019). Trends in polymeric shape memory hydrogels and hydrogel actuators. Polym. Chem. *10*, 1036–1055. https://doi.org/10.1039/c8py01286e.

Shen, M. (2021). A review paper of bio-inspired environmental adaptive and precisely maneuverable soft robots. Preprint at arXiv. https://doi.org/10.48550/arXiv.2101.03171.

Shim, T.S., Kim, S.H., Heo, C.J., Jeon, H.C., and Yang, S.M. (2012). Controlled origami folding of hydrogel bilayers with sustained reversibility for robust microcarriers. Angew. Chem.-Int. Ed. Engl. *51*, 1420–1423. https://doi.org/10.1002/anie.201106723.

Shintake, J., Sonar, H., Piskarev, E., Paik, J., and Floreano, D. (2017). Soft pneumatic gelatin actuator for edible robotics. In 2017 IEEE/RSJ International Conference on Intelligent Robots and Systems (IROS), pp. 6221–6226. https://doi.org/10.1109/IROS.2017.8206525.

Subraveti, S.N., and Raghavan, S.R. (2021). A simple way to synthesize a protective "skin" around Any hydrogel. ACS Appl. Mater. Interfaces *13*, 37645–37654. https://doi.org/10.1021/acsami.1c09460.

Takishima, Y., Yoshida, K., Khosla, A., Kawakami, M., and Furukawa, H. (2021). Fully 3D-printed hydrogel actuator for jellyfish soft robots. ECS J.

Solid State Sci. Technol. *10*, 037002. https://doi.org/10.1149/2162-8777/abea5f.

Wu, B., Jian, Y., Le, X., Lin, H., Wei, S., Lu, W., Zhang, J., Zhang, A., Huang, C.F., and Chen, T. (2019). Supramolecular fabrication of complex 3D hollow polymeric hydrogels with shape and function diversity. ACS Appl. Mater. Interfaces *11*, 48564–48573. https://doi.org/10.1021/acsami.9b17440.

Yu, Y., Yuk, H., Parada, G.A., Wu, Y., Liu, X., Nabzdyk, C.S., Youcef-Toumi, K., Zang, J., and Zhao, X. (2019). Multifunctional "hydrogel skins" on diverse polymers with arbitrary shapes. Adv. Mater. *31*, 1807101. https://doi.org/10.1002/adma.201807101.

Yuk, H., Lin, S., Ma, C., Takaffoli, M., Fang, N.X., and Zhao, X. (2017). Hydraulic hydrogel actuators and robots optically and sonically camouflaged in water. Nat. Commun. *8*, 14230. https://doi.org/10.1038/ncomms14230.

Zhang, M., Li, G., Yang, X., Xiao, Y., Yang, T., Wong, T.W., and Li, T. (2018). Artificial muscle driven soft hydraulic robot: electromechanical actuation and simplified modeling. Smart Mater. Struct. *27*, 095016. https://doi.org/10.1088/1361-665X/aacfe3.

Zhang, C., Zhu, P., Lin, Y., Tang, W., Jiao, Z., Yang, H., and Zou, J. (2020). Fluid-driven artificial muscles: bio-design, manufacturing, sensing, control, and applications. Bio-Des. Manuf. *4*, 123–145. https://doi.org/10.1007/s42242-020-00099-z.

Zhou, S., Wu, B., Zhou, Q., Jian, Y., Le, X., Lu, H., Zhang, D., Zhang, J., Zhang, Z., and Chen, T. (2020). Ionic strength and thermal dual-responsive bilayer hollow spherical hydrogel actuator. Macromol. Rapid Commun. *41*, 1900543. https://doi.org/10.1002/marc.201900543.

Zhu, Q.L., Du, C., Dai, Y., Daab, M., Matejdes, M., Breu, J., Hong, W., Zheng, Q., and Wu, Z.L. (2020). Light-steered locomotion of muscle-like hydrogel by self-coordinated shape change and friction modulation. Nat. Commun. *11*, 5166. https://doi.org/10.1038/s41467-020-18801-1.

STAR★METHODS

KEY RESOURCES TABLE

REAGENT or RESOURCE	SOURCE	IDENTIFIER
Chemicals, peptides, and recombinant proteins		
Gelatin	Aladdin Biochemical Technology Co., Ltd (Shanghai, China)	CAS: 9000-70-8; Lot#G1823014; G108396-500g
Sodium alginate	Aladdin Biochemical Technology Co., Ltd (Shanghai, China)	CAS: 9005-38-3; Lot#J1710035; S100128-500g
Anhydrous calcium chloride	Aladdin Biochemical Technology Co., Ltd (Shanghai, China)	CAS: 10043-52-4; Lot#K1616051; C110766-500g
Acrylamide	Aladdin Biochemical Technology Co., Ltd (Shanghai, China)	CAS: 79-06-1; Lot#E2107072; A108465-500g
N,N′-methylenebisacrylamide	Aladdin Biochemical Technology Co., Ltd (Shanghai, China)	CAS: 110-26-9; Lot#G2002066; M128783-25g
2-Hydroxy-4′-(2-hydroxyethoxy)-2-methylpropiophenone	Aladdin Biochemical Technology Co., Ltd (Shanghai, China)	CAS: 106797-53-9; Lot#L1826109; H137984-100g
Benzophenone	Aladdin Biochemical Technology Co., Ltd (Shanghai, China)	CAS: 119-61-9; Lot#D2114287; B103861-100g
Ethanol anhydrous	Xilong Scientific Co., Ltd. (Guangdong, China)	CAS: 64-17-5
Software and algorithms		
Origin 2018	OriginLab	https://www.originlab.com/
Other		
Ultrapure water system (Synergy)	Merck Millipore	https://www.merckmillipore.com/CN/en
Optical microscope (CKX53)	Olympus	https://www.olympus-ims.com.cn/en/all-products/
Desktop scanning electron microscopy system (Phenom XL)	Phenom Scientific	https://www.phenom-china.com/
Vacuum freeze dryer (Freezon-4.5L)	Labconco	https://www.labconco.com/
Tensile testing machine (Instron 5900)	Instron	https://www.instron.cn/zh-cn/
Programmable syringe pump (LSP10-1B)	Chemyx	https://www.chemyx.com/
Tension tester (HLD-50N)	HANDPI	http://www.handpi.com/
Digital camera (Dino-lite AM4115ZTL)	AnMo Electronics	https://www.dino-lite.com/

RESOURCE AVAILABILITY

Lead contact

Further information and requests for resources and reagents should be directed to and will be fulfilled by the lead contact, Shengli Mi (mi.shengli@sz.tsinghua.edu.cn).

Materials availability

This study did not generate new unique reagents.

Data and code availability

- All data reported in this paper will be shared by the lead contact upon request.
- This paper does not report original code.
- Any additional information required to reanalyze the data reported in this paper is available from the lead contact upon request.

METHOD DETAILS

Materials

Gelatin (~240 g bloom), sodium alginate (Alg, $(C_6H_7O_6Na)_n$, AR), Anhydrous calcium chloride ($CaCl_2$, AR, 96%), Acrylamide (AAm, C_3H_5NO, AR 99.0%), N,N′-methylenebisacrylamide (MBAA, $C_7H_{10}N_2O_2$, 99%), 2-Hydroxy-4′-(2-hydroxyethoxy)-2-methylpropiophenone (Irgacure 2959, $HOCH_2CH_2OC_6H_4COC(CH_3)_2OH$, ≥98.0% (HPLC)), Benzophenone ($C_{13}H_{10}O$, 99%) were purchased from Aladdin Biochemical Technology Co., Ltd (Shanghai, China). Ethanol anhydrous (EtOH, AR) was purchased from Xilong Scientific Co., Ltd. (Guangdong, China). All chemicals were used without further purification. Ultrapure water was obtained using a Synergy ultrapure water system (Merck Millipore).

Characterization of the "hydrogel in situ forming" process

Thickness-time curve

To investigate how to regulate the thickness of the formed thin-walled Alg hydrogels, a simplified planar "hydrogel *in-situ* forming" model (2D) was used. First, anhydrous $CaCl_2$ and gelatin were dissolved in ultrapure water at 65°C. A 10 × 10 mm gelatin layer was prepared by pouring the gelatin solution into a silicone mold and solidifying it at 4 °C for 20 min. The obtained gelatin layers were transferred to another silicone mold. The Alg precursor solution was poured on the gelatin layer and an Alg hydrogel layer formed *in-situ* on the top surface of them at 17 °C. The thickness of the formed Alg hydrogel layers was measured from its cross-sectional microscopy images (CKX53, Olympus). Three groups of samples for each factor were prepared with varied compositions (see Table S1) and three replicates were used for each sample group.

Microscopic morphology by SEM

Cryo-SEM images were obtained using a Phenom XL desktop scanning electron microscopy (SEM) system. The hydrogel sample was frozen in liquid nitrogen and lyophilized using a vacuum freeze dryer (Freezon-4.5L, Labconco). A local section was cut on the freeze-dried sample and then a gold coating was sputtered on it using a vacuum ion sputtering apparatus, before taking the SEM images.

Mechanical test

Tensile tests were performed by using an Instron 5900 tensile testing machine. Dumbbell-shaped samples (40 mm in test length, 4 mm in width, and 1 mm in thickness, as shown in Figure S1) were pulled at a tensile rate of 10 mm/min until they fractured. Their failure strain and failure stress were taken from the fracture point. The tensile modulus took the value of the secant slope in the linear section of the stress–strain curve at 5–10% strain. Three replicates were used for each sample group.

Fabrication of CAUs

Preparation of gelatin cores

Dimensions of cuboid solid gelatin cores were 10 × 10 × 10 mm, and ridge and groove structures (with a width of 2 mm, a depth of 1 mm, and an equilateral triangular shape cross section, as shown in Figure S2.) were designed on each side faces for the formation of crease structures. The gelatin solution (0.1 M Ca^{2+}, 20% w/v gelatin) was transferred to silicone molds and solidified at 4 °C for 20 min to fabricate cuboid solid gelatin cores.

Preparation of the end faces and fluidic connection

AAm-Alg precursor solution (20% w/v AAm as the monomer, 0.2% w/v MBAA as the crosslinker, and 0.2% w/v Irgacure 2959 as the photoinitiator for the PAAm network; 1.5% w/v Alg in ultrapure water) was prepared and then transferred into silicone molds for the 10 × 10 × 2 mm top faces and bottom faces. UV-irradiation (365 nm, appror. 468 mW/cm^2) was performed for 1.5 min at room temperature to crosslink a half-interpenetrating network of the PAAm network with uncrosslinked Alg chains to form the top faces and bottom faces, and to connect the silicone tubes with the top faces. Silicone tubes (1 mm ID/2 mm OD, 0.5 mm ID/1 mm OD) which previously treated with benzophenone (10% w/v in EtOH) for 10 min were used as fluidic connections.

Fabrication process of CAUs

As shown in Figure 2, an assembly of a gelatin core and two end faces was immersed into a Alg precursor solution (1.5% w/v) for 10 min at 17 °C. Then it was transferred into water at 75 °C and a syringe was used to

suck out the melted gelatin through the fluidic connection. During this process, the Alg hydrogels folded in accordance with its predesigned crease pattern and plastic predeformation occurred at the creases. The obtained CAU was transferred into $CaCl_2$ solution (0.1 M) for 1 min to strengthen the connection between the formed Alg hydrogels and the end faces.

Actuation test of CAUs

Actuation curves

The CAUs were actuated under water by pressurized water, which was driven by the preprogrammed injection and withdrawal operations of a programmable syringe pump (Chemyx LSP10-1B). Two digital cameras (Dino-lite AM4115ZTL, ANMO) were arranged in the horizontal and vertical directions to record their actuation in real time. Among them, for measured TCCs, a short-line pointer was marked on their top surface to measure their twisting angle change. Length change of contraction (ΔH) of LCCs, angle change of tilting ($\Delta\beta$) of TBCs, angle change of twisting ($\Delta\theta$) and length change of contraction (ΔH) of TCCs were measured at an injecting and withdrawing rate of 3 mL/min. Three replicates were used for each sample group.

Output force test

The devices and CAU samples for output force tests of CAUs are shown in Figure S3. The tested CAU was actuated at a withdrawing rate of 3 mL/min and the output force (tensile force) generated by the tested CAU was measured by a tension tester (HANDPI HLD-50N) as volume changes per 0.1 mL. Three replicates were used for each sample group.

Combinations of CAUs and fabrication of application demos

The prepared CAUs were first arranged by a silicone mold, and appropriate volume of the AAm-Alg precursor solution was poured into cavities between their end faces, then treated by UV irradiation for 2 min and immersed into $CaCl_2$ solution for 1 min. The actuation tests of CAU combinations and prototypes of grippers were driven by air in the air.

QUANTIFICATION AND STATISTICAL ANALYSIS

Data are represented as mean $\pm$ SD, and Figures were produced by Origin 2018 from the raw data.